

FlexEdit: Marrying Free-Shape Masks to VLLM for Flexible Image Editing

Jue Wang^{1,2*}, Yuxiang Lin^{2,3*}, Tianshuo Yuan¹, Zhi-Qi Cheng⁴,
Xiaolong Wang², Jiao GH¹, Wei Chen¹, Xiaojiang Peng^{2†}

¹Shenzhen Institute of Advanced Technology, Chinese Academy of Sciences

²Shenzhen Technology University ³Georgia Institute of Technology ⁴Carnegie Mellon University

Abstract

Combining Vision Large Language Models (VLLMs) with diffusion models offers a powerful method for executing image editing tasks based on human language instructions. However, language instructions alone often fall short in accurately conveying user requirements, particularly when users want to add, replace elements in specific areas of an image. Luckily, masks can effectively indicate the exact locations or elements to be edited, while they require users to precisely draw the shapes at the desired locations, which is highly user-unfriendly. To address this, we propose FlexEdit, an end-to-end image editing method that leverages both free-shape masks and language instructions for **Flexible Editing**. Our approach employs a VLLM in comprehending the image content, mask, and user instructions. Additionally, we introduce the Mask Enhance Adapter (MEA) that fuses the embeddings of the VLLM with the image data, ensuring a seamless integration of mask information and model output embeddings. Furthermore, we construct FSMI-Edit, a benchmark specifically tailored for free-shape mask, including 8 types of free-shape mask. Extensive experiments show that our method achieves state-of-the-art (SOTA) performance in LLM-based image editing, and our simple prompting technique stands out in its effectiveness. The code and data can be found at https://github.com/A-new-b/flex_edit.

1 Introduction

Image editing has significantly benefited from the exceptional generative capabilities of diffusion models (Li, Singh, and Grover 2023; Chen et al. 2023b; Xuan et al. 2024; Dhariwal and Nichol 2021; Liu, Ding, and Jiang 2023; Rombach et al. 2022a; Geng et al. 2024; Brooks, Holynski, and Efros 2023; Ye et al. 2023; Pan et al. 2024; Zhang et al. 2024). Trained on large scale datasets of text-image pairs, these models can generate high-quality images that align with text prompts. Instruction-based image editing extends these capabilities by using human language instructions to modify specific elements within an original image. However, researchers have found that language instructions can often be ambiguous and complex (Lai et al. 2024; Pi et al. 2023; Huang et al. 2024), thus the text encoders (Radford et al. 2021) fail to accurately represent this information, re-

*These authors contributed equally.

†Corresponding authors.

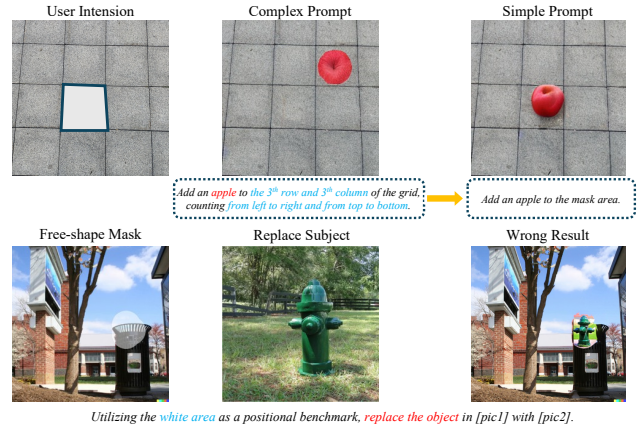
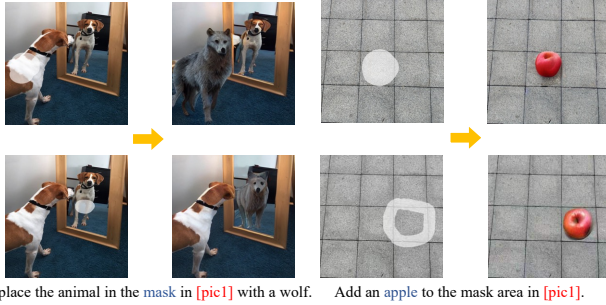


Figure 1: Free-shape mask can simplify the user input when dealing with location related instruction, and more flexible for user input. The compared methods are SmartEdit and Lagen respectively.

sulting in subpar editing outcomes. Large Language Models (LLMs) (Lyu et al. 2019; Ouyang et al. 2022), with their strong instruction-following capabilities, can understand complex human instructions and reason out clear and simple editing directives. Models like SmartEdit (Huang et al. 2024) have pioneered the use of LLMs as text encoders to comprehend complex instructions, allowing users to input complex commands for image editing. However, when it comes to scenarios that are difficult to describe with language, such as specifying precise locations within an image, user have no idea how to prompt the models. Even if the model can understand, such prompts are clearly not user-friendly (e.g., “3th row and 3th column of the grid”).

Users spend excessive time crafting these prompts, and the model may still fail to grasp their meaning, leading to unsatisfactory results (see Upper Figure 1). To address these challenges, visual prompts, such as masks, can effectively and clearly indicate the exact locations or elements to be edited, overcoming the limitations of language commands. However, most existing methods that utilize mask references require users to precisely draw the shapes at the desired locations, which is highly user-unfriendly and can be a barrier to effective use (Chen et al. 2023b). If the mask shapes are irregular or do not completely overlap with the objects, they

(a) Single Image Editing



(b) Multiple Image Editing

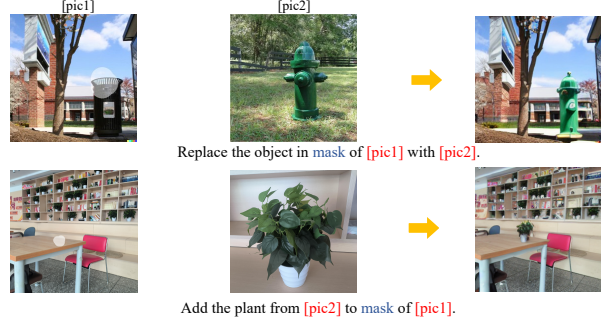


Figure 2: FlexEdit support both (a) single image and (b) multiple image editing, including replace/add an object. The free-shape mask input indicate the localization information, highly user-friendly than asking user to input full mask.

often produce very poor results (see Lower Figure 1).

In real-world scenarios, the shapes users draw for masks are often random and may cover only a small part of the intended area. These free-shape masks challenge the model’s ability to understand user requirements. To address this issue, we created the **Free Shape Mask Instruction Edit (FSIM-Edit)** benchmark, which includes 80 and 125 single images and multiple images respectively, 8 types of free-shape mask. Evaluating existing models with this benchmark revealed that they perform poorly in free-shape mask setting, even after the fine-tuning.

To overcome these issues, we modified the mask functionality in MagicBrush (Zhang et al. 2024), integrating complex instructions with image editing in the FSIM-Edit dataset and proposed FlexEdit, an innovative end-to-end image editing method that leverages both free-shape masks and language instructions for **Flexible Editing (FlexEdit)**. FlexEdit employs a Vision Large Language Model (VLLM) to comprehend the image content, visual prompts, and user instructions. We introduced an adapter structure that fuses the mask represented embeddings of the VLLM with the image data, ensuring a seamless integration of visual information and model output embeddings. This integration enhances the model’s ability to understand and execute complex editing tasks accurately. Experiments demonstrate that FlexEdit significantly outperforms other methods under free-shape mask conditions. Notably, our simple prompting technique proves to be highly effective, setting a new standard for ease of use and precision in the field. FlexEdit represents a significant step forward in the realm of intelligent image editing, combining the strengths of VLLMs and diffusion models to provide a user-friendly and highly capable editing solution.

Our contributions can be summarized as follows:

- We propose FlexEdit, an end-to-end image editing method that combines free-shape masks and language instructions, overcoming the limitations of traditional methods that require precise mask drawing.
- We introduce the Mask Enhanced Adapter (MEA) structure that seamlessly enhance the mask embedding of the Vision Large Language Model (VLLM) with image data, enhancing the model’s ability to understand and execute complex editing tasks.

- We create the Free Shape Mask Instruction Edit (FSIM-Edit) benchmark, which includes a comprehensive dataset with diverse scenarios and editing instructions, to rigorously evaluate the performance of image editing models under free-shape mask conditions.

2 Related Works

In this section, we review the related works in image editing using diffusion models and the advancements in powerful Vision Large Language Models in image editing.

2.1 Image Editing with Diffusion Models

Image editing has achieved exceptional performance thanks to the generative abilities of diffusion models (Brooks, Holynski, and Efros 2023; Zhang et al. 2024; Geng et al. 2024; Chen et al. 2023b; Pan et al. 2024; Ye et al. 2023). Brooks, Holynski, and Efros (2023) introduced Instruct-Pix2Pix, an instruction-based image editing approach that modifies images based on human language instructions. To better align with human instructions, Zhang et al. (2024) proposed MagicBrush, extending text-only instructions to scenarios where a visual mask is provided. On the other hand, subject-driven image editing tasks aim to generate images conditioned on a customized subject and a text prompt that describes the context. For example, Anydoor (Chen et al. 2023b) can teleport target objects to new scenes at user-specified locations (mask) with desired shapes. Pan et al. (2024) proposed Largen for image inpainting that enables seamless inpainting of masked scene images, incorporating both the textual prompts and specified subjects. Singh et al. (2024) and Xuan et al. (2024) start discussing to use coarse visual prompt such as bounding boxes, scribble in guiding the editing, but they use the classic text encoder in diffusion models, which makes it hard to understand those complex instructions.

These models can combine user-provided images with visual prompts, such as masks, to perform image editing. The masks they use need to precisely overlap with the area to be edited, which is not user-friendly. In comparison, we propose using a free-shape mask as a visual prompt and introduce vision large language models (VLLMs) to better under-

stand complex scenarios and instructions for visual prompt-based image editing in an end to end manner.

2.2 VLLMs in Image Editing

Vision Large Language Models (VLLMs) are known for their extensive world knowledge and ability to understand complex instructions (Bai et al. 2023; Lin et al. 2023; Liu et al. 2024, 2023; Li et al. 2023b; Chen et al. 2023a). Fine-tuning these VLLMs for image generation tasks has shown great success in comprehending human language instructions and generating images (Huang et al. 2024; Ge et al. 2024; Li, Singh, and Grover 2023). For example, Huang et al. (2024) fine-tune the LLaVA (Liu et al. 2024) model with dataset of MagicBrush (Zhang et al. 2024) to fit it into the image editing domain. While InstructAny2Pix (Li, Singh, and Grover 2023) build a multi-modal editing system that enables users to edit an image using instructions involving audio, images, and text.

Despite their success, current models predominantly rely on language-based instructions, overlooking the power of visual prompts such as masks. This reliance can limit the intuitiveness and accessibility of the editing process. Our approach seeks to enhance the editing capabilities by incorporating both user instructions and visual prompts, thereby achieving more precise and user-friendly image edits.

3 Methodology

This paper presents *FlexEdit* designed to integrate human instructions and visual prompts for complex image editing tasks. Existing methods, whether based on language instructions or subject mask editing, struggle with understanding user-provided free-shape masks (Chen et al. 2023b; Huang et al. 2024). This challenge lead to a situation that user struggle to draw a mask to meet the models’ need, which is not user-friendly and not acceptable.

In this section, We begin by introducing the FlexEdit Framework and explaining how it integrates free-shape mask with human instructions. We then discuss the Mask Enhanced Adapter (MEA) Module, which plays a crucial role in fusing image features. Finally, we explain the training process for understanding free-shape masks and present the FSMI-Edit Benchmark for evaluating our method.

3.1 FlexEdit Framework

The framework processes three inputs: a scene image x_1 with an associated mask m , a subject image x_2 , and an editing instruction τ . The primary objective is to generate a target image that incorporates x_2 and τ as the content, while utilizing m as a positional reference within x_1 . Importantly, the mask m can take on a free-form shape and does not need to fully overlap with the intended position.

We expanded the vocabulary of LLaVA (Liu et al. 2024) with N new tokens “<img0>, ..., <imgN>” to represent image editing information. As shown in Figure 3, x_1 , x_2 , m , and τ are input into the Vision Large Language Model (VLLM) $V(\cdot; \omega)$ to obtain response tokens r_i . Following this, the response set $R = \{r_1, r_2, \dots, r_n\}$ is processed

to extract the corresponding hidden states $h_i \in \mathcal{H}$, capturing the deeper semantic information from the VLLM’s understanding of the inputs. However, these hidden states primarily reside in the LLM’s text vector space, which poses compatibility challenges when interfacing with the diffusion model—particularly one trained on CLIP (Radford et al. 2021) text embeddings. To address this, we introduce a Q-Former (Li et al. 2023c) module that refines the hidden states into embeddings e compatible with the diffusion model. The transformation process is summarized as follows:

$$\begin{aligned} R &= V(x_1, x_2, \tau, m; \omega) \\ R^t &= \{ \langle \text{img0} \dots \text{imgN} \rangle \} \in R \\ h_i &= H(x_1, x_2, \tau, m; \omega | R_i^t) \\ e &= Q(\mathcal{H}) \end{aligned} \quad (1)$$

where R is the response set, R^t is the set of image tokens, and e represents the embeddings transformed by the Q-Former function Q .

For efficient training, we utilize LoRA (Hu et al. 2021) fine-tuning techniques, freezing most VLLM parameters. Let the ground truth text label of the VLLM response be R' . The VLLM optimization process follows the recurrent loss calculation:

$$\mathcal{L}_{\text{VLLM}}(x, \tau) = - \sum_{\{(x, \tau), R'\}} \log p_{\omega + \Delta\omega(\theta)}(R' | (x, \tau)) \quad (2)$$

where θ represents the LoRA parameters.

Subsequently the Mask Enhanced Adapter (MEA) $A(\cdot; \delta)$ takes embedding e and images x_1, x_2 as input, enhancing the mask feature from the VLLM with scene and subject images. The output c from the MEA UNet block serves as the key and value for cross-attention in the subsequent block recurrently, calculated as:

$$c = A(x_1, x_2, e; \delta) \quad (3)$$

here $A(\cdot; \delta)$ is the MEA function with parameters δ , and c is the MEA UNet block’s output.

During the diffusion process, the encoded image latent $z = \mathcal{E}(x_1)$ is concatenated with the noisy latent z_t and fed into the UNet (Ronneberger, Fischer, and Brox 2015) in a residual manner. The UNet ϵ_α is trained to predict the noise added to the noisy latent z_t , with noise levels increasing under timesteps t , given the condition c from the MEA module. The diffusion optimization process is formulated as:

$$\begin{aligned} \mathcal{L}_{\text{diffusion}} &= \mathbb{E}_{\mathcal{E}(y), \mathcal{E}(x_1), c_T, \epsilon \sim \mathcal{N}(0,1), t} \left[\|\epsilon - \right. \\ &\quad \left. \epsilon_\alpha(t, \text{concat}[z_t, \mathcal{E}(x_1)], c)\|_2^2 \right] \end{aligned} \quad (4)$$

where ϵ is the unscaled noise, t is the sampling step, z_t is the latent noise at step t , $\mathcal{E}(x_1)$ is the encoded scene image, and c is the output from the MEA module.

The overall loss function combines VLLM and diffusion losses:

$$\mathcal{L}_{\text{overall}} = \mathcal{L}_{\text{diffusion}} + \mathcal{L}_{\text{VLLM}} \quad (5)$$

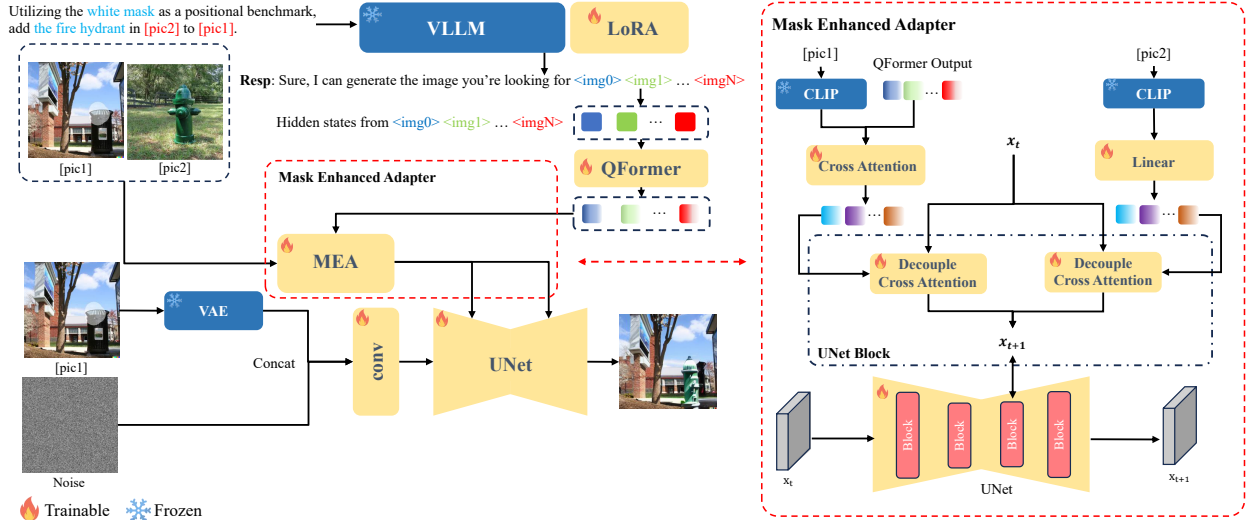


Figure 3: The architecture of the FlexEdit framework. FlexEdit integrates visual prompts and human instructions for complex image editing. It utilizes a VLLM backbone for multi-modal instruction understanding, a Q-Former for refining the hidden states, and a Mask Enhanced Adapter (MEA) for merging image and language model outputs. The final image generation is achieved through a diffusion model.

3.2 Mask Enhanced Adapter

The Mask Enhanced Adapter (MEA) Module aims at fusing the mask editing information from VLLM with the scene and subject images, enhancing the feature for fully interaction. Passing them to the diffusion models allows it to generate the result image for users.

The scene x_1 and subject x_2 images are first mapped to the text embedding space via the CLIP image encoder, for CLIP’s training objective is to maximize the similarity of the image and text label embedding. The output e of QFormer contains the editing intent generated by VLLM after combining the mask and instruction. However, it lacks fine-grained details from the original image. To reintroduce this information, we employed a cross-attention mechanism to fuse the output e from QFormer (Li et al. 2023c) with the features from the scene image x_1 , resulting the scene features f_1 . The key and value of the cross-attention come from the scene image x_1 with the the output e from QFormer as the query. Formulated as follow:

$$f_1 = \text{Softmax} \left(\frac{QK^T}{\sqrt{d}} \right) V \quad (6)$$

where $Q = eW_{q1}$, $K = x_1W_{k1}$, $V = x_1W_{v1}$ are the query, key, and values matrices of the attention operation, and W_{q1} , W_{k1} , W_{v1} are the weight of the trainable linear projection layers.

Considering that the the edited part in final image need to closely resemble a specific object in subject image x_2 , we utilized the linear layer and the decouple cross attention to integrate these features separately, rather than directly fusing them through cross-attention. The subject feature is obtained by mapping the text embedding from x_2 through a linear layer. And then the features f_1 and f_2 go into the UNet block with decouple cross attention where the cross-attention layers. We add a new cross-attention layer for each

cross-attention layer in the UNet block to for features interaction. Finally, given the query features Z , scene features f_1 and subject features f_2 , the output of cross-attention Z' can be defined by the following equation:

$$Z' = \text{Softmax} \left(\frac{QK_1^T}{\sqrt{d}} \right) V_1 + \lambda \text{Softmax} \left(\frac{QK_2^T}{\sqrt{d}} \right) V_2 \quad (7)$$

where $Q = ZW_{q2}$, $K_1 = f_1W_{k2}$, $V_1 = f_1W_{v2}$ and $K_2 = f_2W_{k2}$, $V_2 = f_2W_{v2}$ are the query, key, and values matrices of the attention operation respectively, and W_{q2} , W_{k2} , W_{v2} are the weight matrices of the trainable linear projection layers. λ is weight factor, and we set $\lambda = 0$ when editing single image.

Question: Can you tell me what the masks mean in [pic1]? Apply Purple to the entire object.
 Answer: The masks mean "chair". The visual you requested is <img_0>...<img_N>.



Question: What are the masks in [pic1] representing? Please apply Blue to the entire object.
 Answer: The masks are symbolic of "cat". The visual you requested is <img_0>...<img_N>.



Figure 4: We train model to understand free-shape mask by having it predict the full mask from a given free-form mask. The picture shows two examples of this process.

3.3 Training to Understand Free-Shape Mask

For easy annotation and efficient training, we modified the classical segmentation dataset COCO (Yu et al. 2016) and

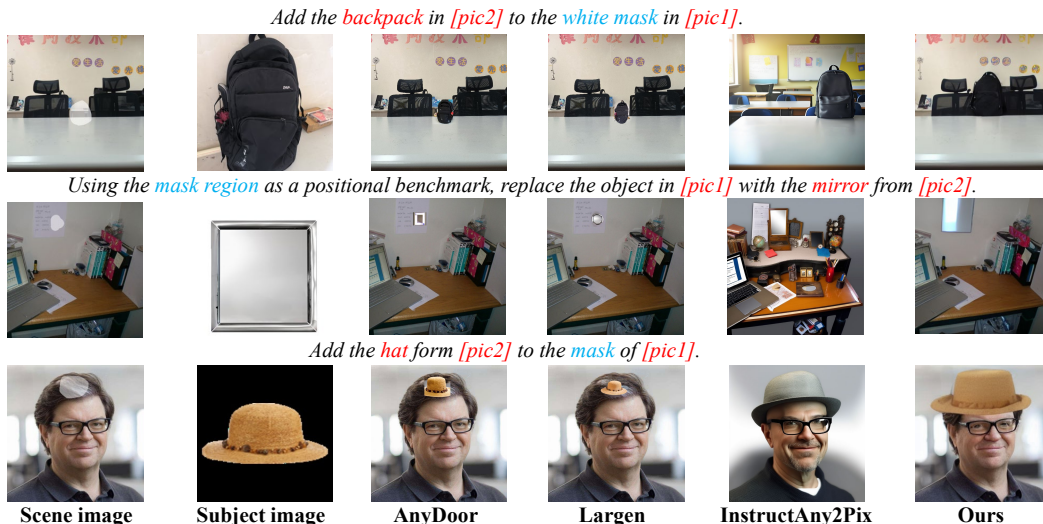


Figure 5: Qualitative results for free-shape mask guided image editing in multiple image setting. We compare the subject image with no background and complex background.

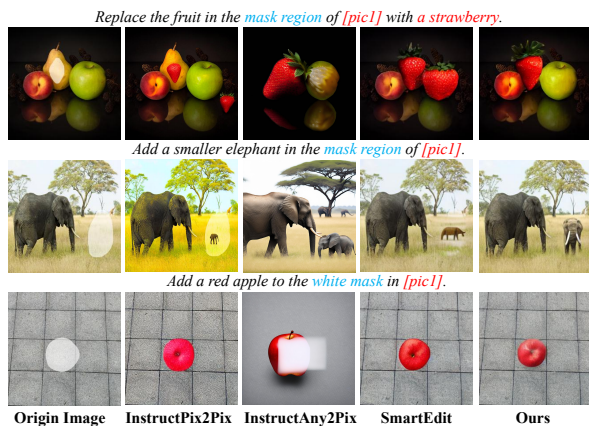


Figure 6: Qualitative results comparison on single image edit.

GRefCOCO (Liu, Ding, and Jiang 2023) for free-shape mask understanding training process. Specifically, we first adapt the original mask label m_o into free-shape mask $m = W(m_o)$ by a simple random walking algorithm W , and model are trained to predict the original mask while output the label of the predict class p . For example, the output can be “The masks means ‘chair’, $\langle img_0 \dots N \rangle$ ”, $\langle img_0 \dots N \rangle$ represent the generate image with original mask m_o (see Figure 4). More technical details will be discussed in the supplementary material.

3.4 FSMI-Edit Benchmark

We construct the **Free-Shape Mask Instruction Edit Benchmark** (FSMI-Edit) for evaluating image editing method in free-shape mask understanding. We focus on daily indoor (e.g. Backpack, Kitchen) and outdoor (e.g. Animals, Ground) scenarios, for subject image we also consider two types of both simple (only subject provided) and complex

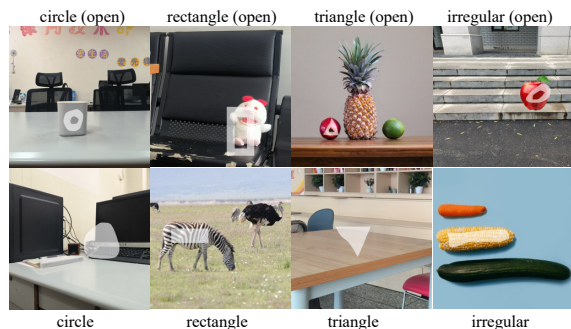


Figure 7: Example of the different types of the free-shape mask from FSMI-Edit benchmark.

(subject with noisy background) subject image. FSMI-Edit consists of 80 and 125 single images and multiple images editing picture respectively.

We carefully design the mask type so that it can mimic human input preference, thoroughly evaluating the performance of free-shape mask reference image editing. Example of the free-shape mask from FSMI-Edit is shown at Figure 7. The free-shape mask consists of 8 type total: *circle*, *circle(open hole)*, *rectangle*, *rectangle (open hole)*, *triangle*, *triangle (open hole)*, *irregular*, *irregular (open hole)* mask, with different orientation. We hope more researchers will pay attention to the free-shape mask guided image editing from these perspectives, thereby fostering the user-friendly multi-modal instruction image editing methods.

4 Experiments

We compare our FlexEdit with SOTA models in both the single and multiple image editing domains. For a fair comparison, we fine-tune the models on the same dataset we use. For models that cannot be fine-tuned, we also report their perfor-

Table 1: Comparison in multiple image editing domain, we compare the results in full mask and free-shape mask setting, and report the scores in foreground and the whole image.

Method	Foreground				Whole Image			
	PSNR \uparrow	CLIP-T \uparrow	CLIP-I \uparrow	DINOv2 \uparrow	PSNR \uparrow	LPIPS \downarrow	CLIP-I \uparrow	DINOv2 \uparrow
<i>Full Mask</i>								
AnyDoor	13.1316	22.0478	<u>0.8959</u>	0.2485	<u>19.2274</u>	<u>0.1055</u>	0.2340	<u>0.9292</u>
Largen	12.5130	20.8105	0.8332	0.2468	18.6747	0.1166	0.2331	0.8886
InstructAny2Pix	8.6129	20.9438	0.7557	0.2424	10.3434	0.5231	0.1723	0.7100
FlexEdit	<u>13.1645</u>	<u>24.1754</u>	0.8279	<u>0.2982</u>	18.0522	0.1433	<u>0.2402</u>	0.8596
<i>Free-Shape Mask</i>								
AnyDoor	11.8483	19.5245	0.7711	0.2451	18.4441	0.1348	0.2280	0.8292
Largen	12.1133	19.1737	0.7627	0.2386	18.6563	0.1373	0.2266	0.8271
InstructAny2Pix	9.6056	20.5750	0.7582	0.2411	11.4099	0.4720	0.1775	0.7151
FlexEdit	12.5648	22.4813	0.7795	0.2908	17.9068	0.1585	0.2353	0.8262

Table 2: Comparison in single image editing domain.

Method	PSNR \uparrow	SSIM \uparrow	LPIPS \downarrow	CLIP-T \uparrow
InstructPix2Pix	19.9414	0.8016	0.1043	20.7010
InstructAny2Pix	15.5149	0.5919	0.2751	20.3758
SmartEdit	21.9535	0.7620	0.0781	20.4910
FlexEdit	22.8081	0.7712	0.0727	20.7081

mance under standard mask settings to assess their ability to understand the content when mask provided.

4.1 Experiments Setting

Training Datasets We include training data from four categories: (1) segmentation datasets, which are modified from COCO and GRefCOCO; (2) image editing datasets, which are adapted from MagicBrush (Zhang et al. 2024), ReasonEdit (Huang et al. 2024), and STRAT (Zhang et al. 2022); (3) in-context visual question answering (VQA) datasets, specifically Mimic-it (Li et al. 2023a), due to its capability of handling multi-image inputs; (4) our self-constructed image editing dataset, which includes a total of 390 pairs of images with complex subject image that should be learned from understand the prompt (e.g. “Add the backpack in [pic2] to the white mask in [pic1]” see Figure 5).

To address the imprecision of user-drawn masks in real-world applications, we avoid using the actual masks directly as inputs. Instead, we simulate user input by generating free shape masks using random walks on the real masks. These generated masks are then reviewed and re-annotated by three volunteers to ensure they closely mimic real-life user inputs. For the segmentation datasets, the model’s objective is to re-generate masks based on the free-form input to match the ground truth shapes. Training on the VQA dataset ensures that the model retains its analytical and reasoning capabilities during fine-tuning. Additional technical details can be found in the supplementary materials.

Metrics The final objective for the model is to focus understand the free-shape mask area during editing, adhering to the instructions while minimizing changes to the overall image. To assess the ability in the mask understanding,

we modified the mask-evaluate setting. Unlike the setting of aforementioned methods that use the mask area in evaluating the generate quality, given that free-shape masks’ imprecise nature, we use the real edited regions from the GT as the evaluate masks instead of the input one. In thoroughly assessing the quality of image editing, we split the metric into the single and multiple image evaluation:

Multiple Image: We include PSNR, CLIP-T, CLIP-I (Radford et al. 2021), and DINOv2 (Oquab et al. 2023) for the metric of foreground quality assessing, where CLIP-T measures how performance of the edited foreground aligns with the text label. PSNR, CLIP-I and DINOv2 assess the visual similarity between the generated images and the GT foreground images. LPIPS was introduced in the whole image evaluation while CLIP-T is excluded since CLIP-T label can not be annotated in the whole image setting.

Single Image: For single-image editing, in line with SmartEdit (Huang et al. 2024), we use PSNR, SSIM, LPIPS to evaluate background similarity, and CLIP-T to assess the alignment of the results’ foreground with the text label.

4.2 Comparisons with SOTA models

Baselines We compared the diffusion only method AnyDoor and Largen, as well as the VLLM plus diffusion method instructAny2Pix, with our method in multiple image editing. Here, AnyDoor and Largen are the methods designed for zero-shot subject-driven image editing task, generating appropriate objects from the subject image within the masked area of the scene image. InstructAny2Pix leverages a VLLM to combine multiple user images and text instructions for editing the corresponding images.

For single image editing, we compare FlexEdit with InstructPix2Pix, InstructAny2Pix, and SmartEdit. Instruct-Pix2Pix and SmartEdit edit images based on human language instructions. InstructPix2Pix uses a CLIP structure to understand human instructions and image content, while SmartEdit employs a large visual language model to interpret human instructions and image content.

Multiple Image Editing We first provide a qualitative comparison between FlexEdit with other method with add/replace operation and simple/complex subject images in

Table 3: Ablation study in multiple image editing. We evaluate the ‘CA’, standing for cross attention in MEA, and ‘DCA’, standing for decouple cross attention.

CA	DCA	Foreground				Whole Image			
		PNSR \uparrow	CLIP-T \uparrow	CLIP-I \uparrow	DINOv2 \uparrow	PNSR \uparrow	LPIPS \downarrow	CLIP-I \uparrow	DINOv2 \uparrow
✓	✓	12.5794	22.4391	0.7796	0.2890	17.9068	0.1585	0.2353	0.8262
-	✓	12.1836	21.6230	0.7451	0.2846	17.5058	0.1806	0.2378	0.8140
✓	-	11.8367	21.3692	0.7561	0.2799	17.0976	0.1813	0.2341	0.8124

Table 4: Ablation study in single image editing, same setting as experiment in multiple image editing.

CA	DCA	PSNR \uparrow	SSIM \uparrow	LPIPS \downarrow	CLIP-T \uparrow
✓	✓	22.8081	0.7712	0.0727	20.7081
-	✓	21.8579	0.7546	0.0931	19.8630
✓	-	20.4195	0.7230	0.1186	19.8566

Figure 5. The compared model either fail to understand the free-shape mask (AnyDoor, Largen), or unintentionally change the background image (InstructAny2Pix).

Foreground Quality Comparison: Under the normal mask setting, the AnyDoor and Largen shows the best score in CLIP-I, indicating the exhibit of the highest similarity to the foreground GT image, whereas InstructAny2Pix is less than ours. DINOv2 shows the same trend as CLIP-I, except ours FlexEdit achieved 0.2982, marginly higher than others. For the CLIP-T scores which represented the similarity between the generated foreground and the text label, however, FlexEdit achieved 24.1754, achieving the SOTA results. In the free mask setting, where user-provided masks are more arbitrary and abstract, methods like AnyDoor and Largen, which generate images only within the mask, fail to meet user expectations, resulting in a significant drop in metrics. InstructAny2Pix’s performance do not decrease and perform stable in this setting. In this setting, our model have a sightly performance drop, while achieve the state-of-the-art results among all the metrics, showing our strong ability in understanding the free-shape mask. The detail results can be found at Table 1 (Foreground Image).

Whole Image Quality Comparison: The PNSR, CLIP-I, DINOv2 is close in the whole image setting for AnyDoor, Largen and FlexEdit. Note that InstructAny2Pix perform marginly bad at this setting, indicating that it will modify the unintentional background image, this is a long-stand problem in an end-to-end diffusion generation framework. However, our FlexEdit while edit the foreground object well, keeping the whole image stable, demonstrating our model’s strong image understanding and image edting abilities. More detail results can be found at Table 1 (Whole Image).

Single Image Editing For a fair comparison, we fine-tune InstructPix2Pix and SmartEdit under the same setting as ours¹. The qualitative comparison is shown in Figure 6,

¹InstructAny2Pix has not released the training code at the time this paper submitted.

InstructAny2Pix can understand the free-shape mask, while will change the background image unintentionally. SmartEdit works better than InstructPix2Pix for it can understand the mask occasionally, instructionPix2Pix however, shows bad performance among the three methods.

Results shows that InstructPix2Pix performs bad even after fine-tuning, we argue that these can come from the problem that CLIP simple encoder can not fully understand the free-shape mask. InstrucAny2Pix still suffers from it can not maintain the whole image during the editing process. FlexEdit in the other hand, understand the free-shape mask and keep the rest of the image still, this can come from our MEA module for its ability in information extraction. SmartEdit shares the similar result as ours, with a sightly weakness that can come from our single-multiple image mixed training strategy. Detail results can be found at Table 2. More comparison can be found in the supplementary material.

4.3 Ablation study on MEA

We designed two different structures and compared their performance metrics in both single image and multiple image editing to validate the effectiveness of each module within the adapter. First, we remove the Cross Attention (CA) layer and directly used the output of the QFormer as the scene feature input into the following decouple cross attention, without the scene picture interaction. We also change the Decouple Cross Attention (DCA) structure with a general cross attention and examine the MEA effectiveness in image fusion. As shown in Table 3, in multiple image editing, the CA and DCA can help boost the model performance, both seperately and jointly. For single image editing, as shown in Table 4, though the MEA module does not work in this mode, it can learn during the joint training process, and CA, DCA involving shows a better result for the single image performance.

5 Conclusion

In this paper, we introduce FlexEdit, an end-to-end method based on Visual Language Models (VLLM) for free shape mask guided image editing. Our model addresses the challenge of imprecise and irregular mask shapes drawn by humans by incorporating free shape masks during the training process. To achieve effective image fusion, we propose a Mask Enhanced Adapter (MEA), which enhanced the mask embedding from the VLLM with image data for seamless blending. To support the image editing community, we also

develop FSMI-Edit, a new evaluation dataset specifically designed for free shape mask scenarios. Our method achieves state-of-the-art results on the FSMI-Edit benchmark, outperforming other models trained under similar conditions, whether in free shape mask or full-mask settings.

References

- Aminabadi, R. Y.; Rajbhandari, S.; Awan, A. A.; Li, C.; Li, D.; Zheng, E.; Ruwase, O.; Smith, S.; Zhang, M.; Rasley, J.; et al. 2022. Deepspeed-inference: enabling efficient inference of transformer models at unprecedented scale. In *SC22: International Conference for High Performance Computing, Networking, Storage and Analysis*, 1–15. IEEE.
- Bai, J.; Bai, S.; Yang, S.; Wang, S.; Tan, S.; Wang, P.; Lin, J.; Zhou, C.; and Zhou, J. 2023. Qwen-vl: A frontier large vision-language model with versatile abilities. *arXiv preprint arXiv:2308.12966*.
- Brooks, T.; Holynski, A.; and Efros, A. A. 2023. Instruct-pix2pix: Learning to follow image editing instructions. In *Proceedings of the IEEE/CVF Conference on Computer Vision and Pattern Recognition*, 18392–18402.
- Chen, J.; Zhu, D.; Shen, X.; Li, X.; Liu, Z.; Zhang, P.; Krishnamoorthi, R.; Chandra, V.; Xiong, Y.; and Elhoseiny, M. 2023a. Minigt-v2: large language model as a unified interface for vision-language multi-task learning. *arXiv preprint arXiv:2310.09478*.
- Chen, X.; Huang, L.; Liu, Y.; Shen, Y.; Zhao, D.; and Zhao, H. 2023b. Anydoor: Zero-shot object-level image customization. *arXiv preprint arXiv:2307.09481*.
- Dhariwal, P.; and Nichol, A. 2021. Diffusion models beat gans on image synthesis. *Advances in neural information processing systems*, 34: 8780–8794.
- Ge, Y.; Zhao, S.; Zhu, J.; Ge, Y.; Yi, K.; Song, L.; Li, C.; Ding, X.; and Shan, Y. 2024. Seed-x: Multimodal models with unified multi-granularity comprehension and generation. *arXiv preprint arXiv:2404.14396*.
- Geng, Z.; Yang, B.; Hang, T.; Li, C.; Gu, S.; Zhang, T.; Bao, J.; Zhang, Z.; Li, H.; Hu, H.; et al. 2024. Instructdiffusion: A generalist modeling interface for vision tasks. In *Proceedings of the IEEE/CVF Conference on Computer Vision and Pattern Recognition*, 12709–12720.
- Hu, E. J.; Shen, Y.; Wallis, P.; Allen-Zhu, Z.; Li, Y.; Wang, S.; Wang, L.; and Chen, W. 2021. Lora: Low-rank adaptation of large language models. *arXiv preprint arXiv:2106.09685*.
- Huang, Y.; Xie, L.; Wang, X.; Yuan, Z.; Cun, X.; Ge, Y.; Zhou, J.; Dong, C.; Huang, R.; Zhang, R.; et al. 2024. Smartedit: Exploring complex instruction-based image editing with multimodal large language models. In *Proceedings of the IEEE/CVF Conference on Computer Vision and Pattern Recognition*, 8362–8371.
- Lai, X.; Tian, Z.; Chen, Y.; Li, Y.; Yuan, Y.; Liu, S.; and Jia, J. 2024. Lisa: Reasoning segmentation via large language model. In *Proceedings of the IEEE/CVF Conference on Computer Vision and Pattern Recognition*, 9579–9589.
- Li, B.; Zhang, Y.; Chen, L.; Wang, J.; Pu, F.; Yang, J.; Li, C.; and Liu, Z. 2023a. Mimic-it: Multi-modal in-context instruction tuning. *arXiv preprint arXiv:2306.05425*.
- Li, B.; Zhang, Y.; Chen, L.; Wang, J.; Yang, J.; and Liu, Z. 2023b. Otter: A Multi-Modal Model with In-Context Instruction Tuning. *arXiv preprint arXiv:2305.03726*.
- Li, J.; Li, D.; Savarese, S.; and Hoi, S. 2023c. Blip-2: Bootstrapping language-image pre-training with frozen image encoders and large language models. In *International conference on machine learning*, 19730–19742. PMLR.
- Li, S.; Singh, H.; and Grover, A. 2023. InstructAny2Pix: Flexible Visual Editing via Multimodal Instruction Following. *arXiv preprint arXiv:2312.06738*.
- Lin, B.; Zhu, B.; Ye, Y.; Ning, M.; Jin, P.; and Yuan, L. 2023. Video-llava: Learning united visual representation by alignment before projection. *arXiv preprint arXiv:2311.10122*.
- Liu, C.; Ding, H.; and Jiang, X. 2023. Gres: Generalized referring expression segmentation. In *Proceedings of the IEEE/CVF conference on computer vision and pattern recognition*, 23592–23601.
- Liu, H.; Li, C.; Li, Y.; and Lee, Y. J. 2023. Improved baselines with visual instruction tuning. *arXiv preprint arXiv:2310.03744*.
- Liu, H.; Li, C.; Wu, Q.; and Lee, Y. J. 2024. Visual instruction tuning. *Advances in neural information processing systems*, 36.
- Loshchilov, I.; and Hutter, F. 2017. Decoupled weight decay regularization. *arXiv preprint arXiv:1711.05101*.
- Lyu, H.; Sha, N.; Qin, S.; Yan, M.; Xie, Y.; and Wang, R. 2019. Advances in neural information processing systems. *Advances in neural information processing systems*, 32.
- Oquab, M.; Darcet, T.; Moutakanni, T.; Vo, H.; Szafraniec, M.; Khalidov, V.; Fernandez, P.; Haziza, D.; Massa, F.; El-Nouby, A.; et al. 2023. Dinov2: Learning robust visual features without supervision. *arXiv preprint arXiv:2304.07193*.
- Ouyang, L.; Wu, J.; Jiang, X.; Almeida, D.; Wainwright, C.; Mishkin, P.; Zhang, C.; Agarwal, S.; Slama, K.; Ray, A.; et al. 2022. Training language models to follow instructions with human feedback. *Advances in neural information processing systems*, 35: 27730–27744.
- Pan, Y.; Mao, C.; Jiang, Z.; Han, Z.; and Zhang, J. 2024. Locate, Assign, Refine: Taming Customized Image Inpainting with Text-Subject Guidance. *arXiv preprint arXiv:2403.19534*.
- Pi, R.; Gao, J.; Diao, S.; Pan, R.; Dong, H.; Zhang, J.; Yao, L.; Han, J.; Xu, H.; Kong, L.; et al. 2023. Detgpt: Detect what you need via reasoning. *arXiv preprint arXiv:2305.14167*.
- Radford, A.; Kim, J. W.; Hallacy, C.; Ramesh, A.; Goh, G.; Agarwal, S.; Sastry, G.; Askell, A.; Mishkin, P.; Clark, J.; et al. 2021. Learning transferable visual models from natural language supervision. In *International conference on machine learning*, 8748–8763. PMLR.
- Rombach, R.; Blattmann, A.; Lorenz, D.; Esser, P.; and Ommer, B. 2022a. High-resolution image synthesis with latent diffusion models. In *Proceedings of the IEEE/CVF conference on computer vision and pattern recognition*, 10684–10695.

Rombach, R.; Blattmann, A.; Lorenz, D.; Esser, P.; and Ommer, B. 2022b. High-Resolution Image Synthesis With Latent Diffusion Models. In *Proceedings of the IEEE/CVF Conference on Computer Vision and Pattern Recognition (CVPR)*, 10684–10695.

Ronneberger, O.; Fischer, P.; and Brox, T. 2015. U-net: Convolutional networks for biomedical image segmentation. In *Medical image computing and computer-assisted intervention—MICCAI 2015: 18th international conference, Munich, Germany, October 5-9, 2015, proceedings, part III 18*, 234–241. Springer.

Singh, J.; Zhang, J.; Liu, Q.; Smith, C.; Lin, Z.; and Zheng, L. 2024. SmartMask: Context Aware High-Fidelity Mask Generation for Fine-grained Object Insertion and Layout Control. In *Proceedings of the IEEE/CVF Conference on Computer Vision and Pattern Recognition*, 6497–6506.

Xuan, W.; Xu, Y.; Zhao, S.; Wang, C.; Liu, J.; Du, B.; and Tao, D. 2024. When ControlNet Meets Inexplicit Masks: A Case Study of ControlNet on its Contour-following Ability. *arXiv preprint arXiv:2403.00467*.

Ye, H.; Zhang, J.; Liu, S.; Han, X.; and Yang, W. 2023. Ip-adapter: Text compatible image prompt adapter for text-to-image diffusion models. *arXiv preprint arXiv:2308.06721*.

Yu, L.; Poirson, P.; Yang, S.; Berg, A. C.; and Berg, T. L. 2016. Modeling context in referring expressions. In *Computer Vision—ECCV 2016: 14th European Conference, Amsterdam, The Netherlands, October 11-14, 2016, Proceedings, Part II 14*, 69–85. Springer.

Zhang, B.; Liu, Y.; Lu, K.; Niu, L.; and Zhang, L. 2022. Spatial Transformation for Image Composition via Correspondence Learning. *arXiv preprint arXiv:2207.02398*.

Zhang, K.; Mo, L.; Chen, W.; Sun, H.; and Su, Y. 2024. Magicbrush: A manually annotated dataset for instruction-guided image editing. *Advances in Neural Information Processing Systems*, 36.

Zheng, L.; Chiang, W.-L.; Sheng, Y.; Zhuang, S.; Wu, Z.; Zhuang, Y.; Lin, Z.; Li, Z.; Li, D.; Xing, E.; et al. 2024. Judging llm-as-a-judge with mt-bench and chatbot arena. *Advances in Neural Information Processing Systems*, 36.

A Implementation Details

A.1 Training details

The LLaVA v1.1-7B (Liu et al. 2024) and QFormer (Li et al. 2023c) pretrained by SmartEdit (Huang et al. 2024) and the Stable Diffusion-1.5 (Rombach et al. 2022b) are the VLLM and diffusion model pretrained weights. The base LLM for LLaVA1.1-7B is Vicuna-7B (Zheng et al. 2024). FlexEdit is trained for 12000 steps on 4 NVIDIA A100 GPUs with batch size 4 and gradient accumulation 8, using AdamW (Loshchilov and Hutter 2017) optimizer with 1×10^{-5} learning rate. Number N of image new tokens is set to 32.

For the fine-tuning process, we employed DeepSpeed (Aminabadi et al. 2022) Zero-2 to perform LoRA (Hu et al. 2021) fine-tuning with the following parameters: LoRA Rank = 8, LoRA Alpha = 16, and LoRA Dropout = 0.05.

The base model is frozen and the LoRA fine-tuning target modules are query project layers and value project layers.

A.2 Data Construction Pipeline

In this section, we present detail methodology of the FSMI-Edit benchmark and the benchmark data construction pipeline.

Multiple images editing datasets construction pipeline

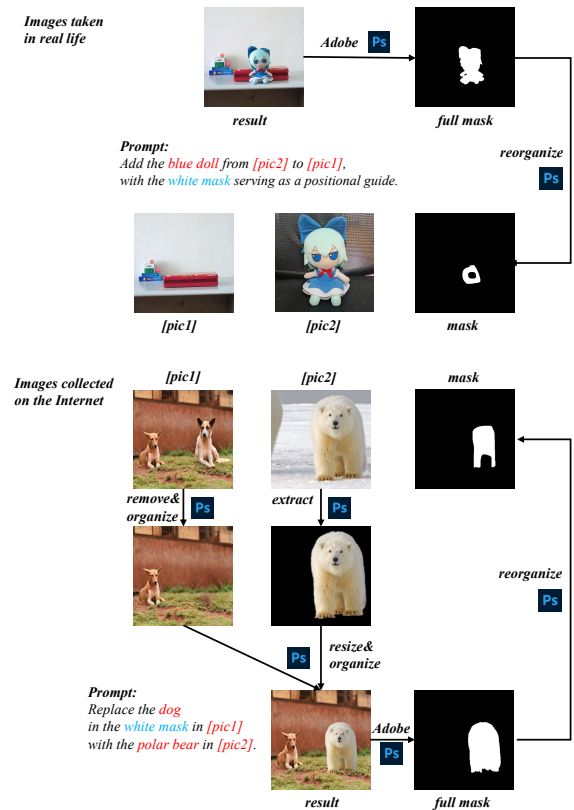


Figure 8: In the multiple images editing datasets creation process, we use Adobe Photoshop to extract the full mask from the result image, then redraw the mask in different shape, and write prompts based on the task to serve as input instructions.

To enable FlexEdit to handle complex scenes, intricate instructions, and free-shape mask editing, we have designed a data construction pipeline to build the self-construction dataset used in training and FSMI-Edit benchmark. These dataset and benchmark primarily include everyday items, indoor objects, and outdoor scenes. We have carefully designed eight types of free-shape masks to simulate user input preferences (e.g. casually and unprecisely), allowing for a more accurate evaluation of free-shape mask-based image editing performance.

The images in the benchmark come from real-world photography and internet sources. Images captured in real life are cropped to a suitable size to meet the benchmark requirements. Images collected from the internet have variations in

Single image editing datasets construction pipeline

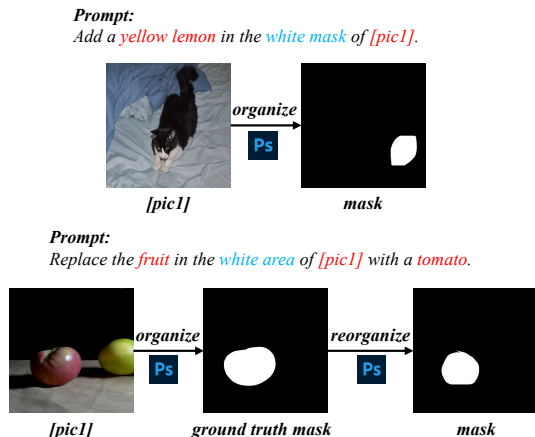


Figure 9: In the single image editing datasets creation process, we use Adobe Photoshop to draw different shaped masks in specified areas of the scene image [pic1] based on the task requirements. Then we write prompts based on the task to serve as input instructions.

saturation, contrast, and other parameters, which could affect the image editing results. To rectify this, we use Adobe Photoshop¹ to process these images and obtain more harmonious images. Additionally, Adobe Photoshop integrates a segmentation model, allowing for direct segmentation operations during image processing. Combined with Adobe Photoshop’s AI filling technology, it can process images more conveniently and improve work efficiency. Therefore, we use Adobe Photoshop to prepare the benchmark.

In the benchmark, we mark the captured or collected scene images as [pic1], the object images as [pic2], the prompts written according to task requirements as prompt, and the various drawn shapes of masks as mask. The creation of the multiple images editing datasets is divided into two parts: images captured in real-life scenarios and images collected from the internet.

For images captured in real-life, tasks are completed by moving, placing, etc. to accomplish task requirements. Then we use Adobe Photoshop to extract the complete mask of specific objects from the images. On these complete masks, we draw eight free-shape masks that conform to user input habits, such as circles, rectangles, triangles, irregular shapes, and their hollow versions. Finally, we write prompts based on the task requirements to complete the dataset creation.

For images collected from the internet, The images collected on the Internet take the dog and polar bear in Figure 1 as an example. We use Adobe Photoshop to remove the dog on the right side of the scene image [pic1] and fill in the background to obtain the final scene image. Subsequently, we use the integrated segmentation model to extract the polar bear from the object image [pic2], then process the polar bear and fuse it into the scene image for further optimization. The extracted mask is drawn to obtain masks of dif-

¹<https://www.photoshop.com/>

ferent shapes. Finally, prompts are written according to the task description. The creation of the multiple images editing benchmark are completed.

Similarly, in the single image editing benchmark, we use Adobe Photoshop to draw free-shape masks in specified locations according to the task requirements, and prompts are written based on the task.

The data production pipeline is illustrated in Figure 8 and Figure 9. Figure 1 shows the production pipeline of the multiple images editing benchmark, and Figure 2 shows the production pipeline of the single image editing benchmark. The images of our benchmark come from images taken in the real world (such as the blue doll in Figure 1) and images collected from the Internet (such as the polar bear and dogs in Figure 1). Our benchmark tasks are divided into two categories: Add and Replace. For example, in Figure 1, the tasks include: “Add the blue doll from [pic2] to [pic1], with the white mask serving as a positional guide” and “Replace the dog in the white mask in [pic1] with the polar bear in [pic2]”. In Figure 2, the tasks include: “Add a yellow lemon in the white mask of [pic1]” and “Replace the fruit in the white area of [pic1] with a tomato”.

A.3 Dataset Composition

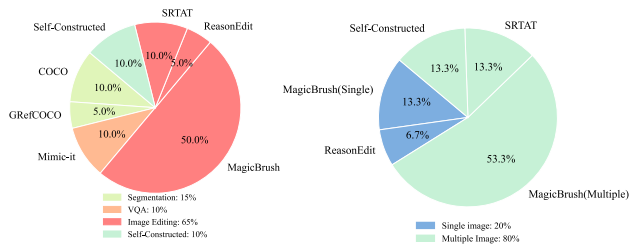


Figure 10: This pie chart illustrates the input distribution of datasets during the training process. The first chart shows the proportion of four different datasets used in training, while the second chart indicates the proportion of single-image versus multi-image inputs within the image editing dataset.

During the training process, we employed a mixed training approach, using four different datasets as input with specific probability ratios. As shown in Figure 10, the segmentation datasets modified from COCO and GRefCOCO account for 15%, the VQA dataset Mimic-it (Li et al. 2023a) accounts for 10%, the image editing datasets adapted from MagicBrush (Zhang et al. 2024), ReasonEdit (Huang et al. 2024), and STRAT (Zhang et al. 2022) account for 65%, and our self-constructed image editing dataset account for 10%. Within the whole image editing datasets, single-image editing tasks made up 20%, while multi-image editing tasks comprised 80%.

B Qualitative comparisons

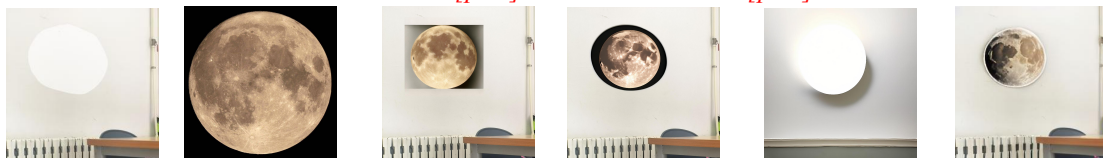
In this section, we provide a qualitative comparison between FlexEdit with other method on 8 different types in FSMI-Edit Benchmark. The multiple images comparisons

multi-images
(circle)

Add the **backpack** in [pic2] to the **white mask** in [pic1].



Add the **moon** in [pic2] to the **white mask** in [pic1].



multi-images
(circle open)

Replace the **yellow chili** in the **white mask** of [pic1] with the **cat** in [pic2].

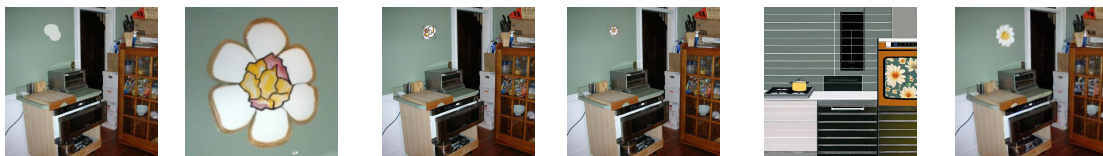


Replace the **doll** in the **white mask** of [pic1] with the **backpack** in [pic2].

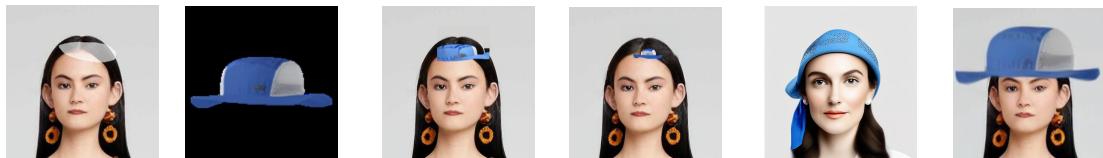


multi-images
(irregular)

Employing the **white mask** as a position marker, add the **flowers** from [pic2] to [pic1].

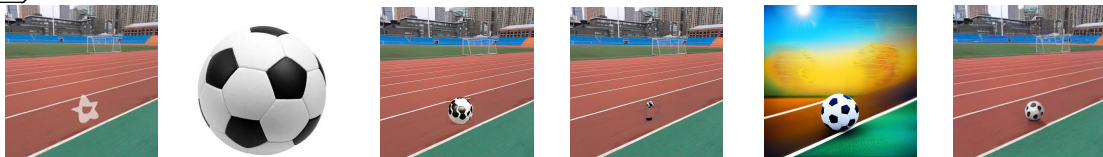


Add the **hat** form [pic2] to the **white mask** of [pic1].



multi-images
(irregular open)

Add the **football** in [pic2] to the **white mask** in [pic1].



Add the **hat** form [pic2] to the **white mask** of [pic1].



Scene image

Subject image

AnyDoor

Largen

InstructAny2Pix

Ours

Figure 11: Multiple images editing comparison on circle mask, circle open mask, irregular mask, irregular open mask.

multi-images
(rectangle)

Add the **bag** in [pic2] to the **white mask** of [pic1].



Applying the **white mask** as a position guide, replace the **yellow ball** in [pic1] with the white **golf ball** from [pic2].



multi-images
(rectangle open)

Replace the **basketball** in the **white mask** of [pic1] with the **bag** in [pic2].



Replace the **bicycle** in [pic1] with the **motorcycle** from [pic2], using the **white mask** as a position reference.



multi-images
(triangle)

Replace the **cake** in the **white mask** in [pic1] with the **apple** in [pic2].

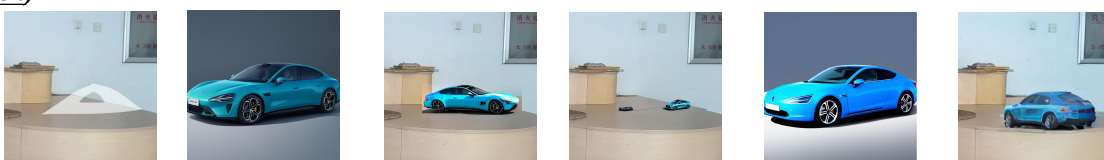


Add the **cake** in [pic2] to the **white mask** in [pic1].



multi-images
(triangle open)

Add the **blue car** in [pic2] to the **white mask** in [pic1].



Replace the **sheep** in the **white mask** in [pic1] with the **horse** in [pic2].

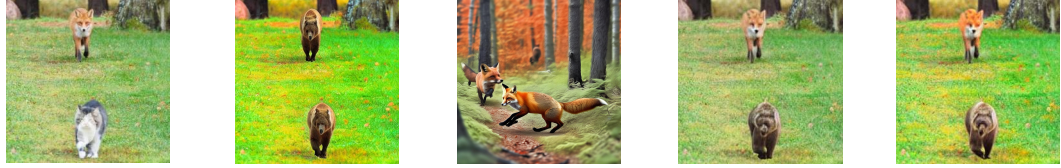


Scene image Subject image AnyDoor Largen InstructAny2Pix Ours

Figure 12: Multiple images editing comparison on rectangle mask, rectangle open mask, triangle mask, triangle open mask.

*single-image
(circle)*

Replace the animal in the *white mask* of [pic1] with *a bear*.

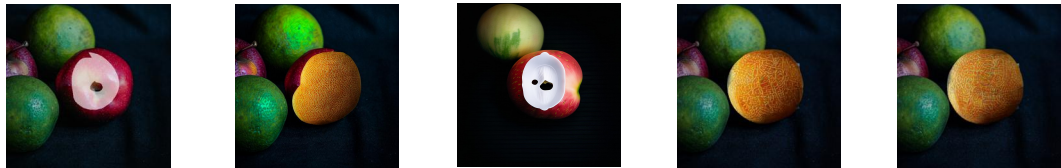


Replace the animal in the *white mask* of [pic1] with *an elephant*.



*single-image
(circle open)*

Replace the fruit in the *white mask* of [pic1] with *a melon*.



Replace the animal in the *white mask* of [pic1] with *a goat*.



*single-image
(irregular)*

Replace the vegetable in the *white mask* of [pic1] with *a chili*.

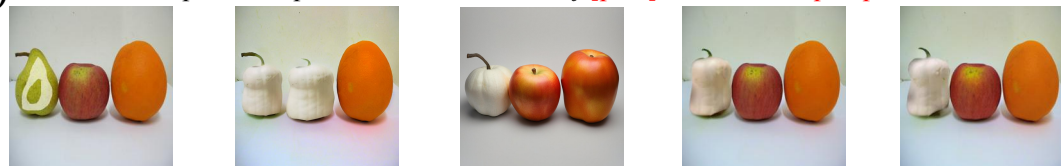


Replace the fruit in the *white mask* of [pic1] with *a litchi*.



*single-image
(irregular open)*

Replace the pear in the *white mask* of [pic1] with *a white pumpkin*.



Replace the vegetable in the *white mask* of [pic1] with *a pitaya*.



Origin Image

InstructPix2Pix

InstructAny2Pix

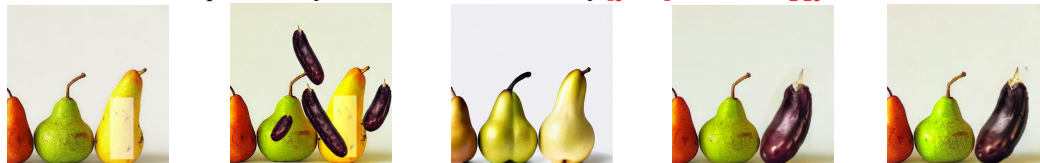
SmartEdit

Ours

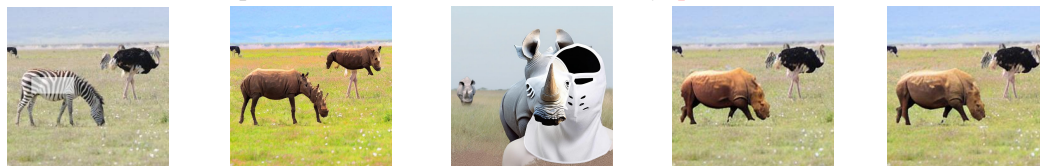
Figure 13: Single image editing comparison on circle mask, circle open mask, irregular mask, irregular open mask.

*single-image
(rectangle)*

Replace the fruit in the *white mask* of [pic1] with *an eggplant*.

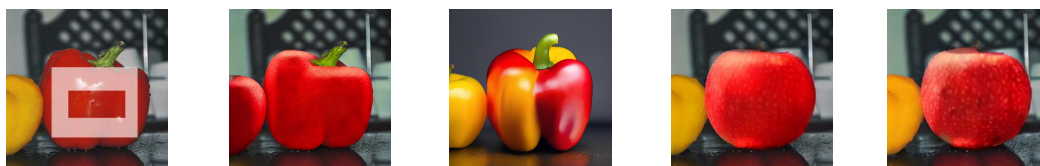


Replace the animal in the *white mask* of [pic1] with *a rhino*.

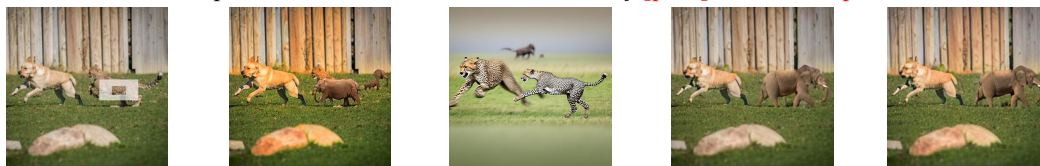


*single-image
(rectangle open)*

Replace the vegetable in the *white mask* of [pic1] with *an apple*.

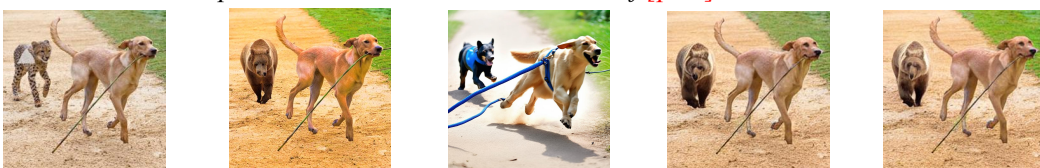


Replace the animal in the *white mask* of [pic1] with *an elephant*.



*single-image
(triangle)*

Replace the animal in the *white mask* of [pic1] with *a bear*.

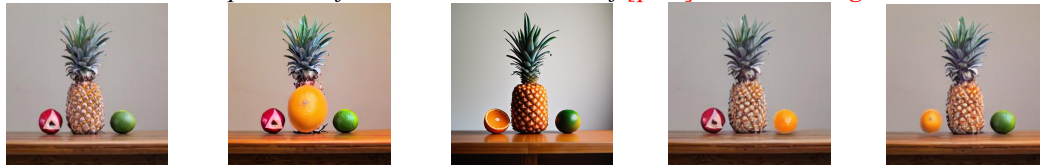


Replace the animal in the *white mask* of [pic1] with *a squirrel*.



*single-image
(triangle open)*

Replace the fruit in the *white mask* of [pic1] with *an orange*.



Replace the fruit in the *white mask* of [pic1] with *a peach*.



Origin Image

InstructPix2Pix

InstructAny2Pix

SmartEdit

Ours

Figure 14: Single images editing comparison on rectangle mask, rectangle open mask, triangle mask, triangle open mask.

are shown in Figure 11 and Figure 12. The single image comparisons are shown in Figure 13 and Figure 14.

There are two situations for multiple models on the benchmark: one where the mask closely matches with the subject, and another where the mask and subject are less well-matched.

Some of the compared models either alter the background image (as seen with InstructAny2Pix) or change the size of the object (as seen with Anydoor and Largen), leading to a decrease in visual quality. For example, in the first row of Figure 5, the user’s task is to add the bag in [pic2] to the white mask in [pic1], Anydoor and Largen generate the bag within the masked area, resulting in a bag size that is inconsistent with the user’s specifications. InstructAny2Pix, on the other hand, alters the overall image style. In contrast, our FlexEdit integrates the specified bag into the designated position in the scene with an appropriate size. The visual quality of the images generated by FlexEdit is superior to that of the other models.

If the mask does not match well with the subject, particularly when there are hollows in the mask shape, the compared models either fail to interpret the free-shape mask correctly (such as InstructPix2Pix), alter the background image, or only generate images within the masked area (as seen with Anydoor Largen). Specifically, in the third row of Figure 5, the user’s task is to replace the basketball in [pic1] with the bag in [pic2], Anydoor generates the bag within the mask area, Largen fails to understand the free-shape mask, and InstructAny2Pix alters the overall image style. In contrast, our FlexEdit model preserves the background and replaces the basketball with the bag in the scene, maintaining the correct size and positioning. This further highlights the strong free-shape mask interpretation and image editing capabilities of our FlexEdit model.